01 Feb 2001

FDTD and Experimental Investigation of EMI from Stacked-Card PCB Configurations

David M. Hockanson

Xiaoning Ye

James L. Drewniak
Missouri University of Science and Technology, drewniak@mst.edu

Todd H. Hubing
Missouri University of Science and Technology

et. al. For a complete list of authors, see https://scholarsmine.mst.edu/ele_comeng_facwork/1627

FDTD and Experimental Investigation of EMI from Stacked-Card PCB Configurations

David M. Hockanson, *Member, IEEE*, Xiaoning Ye, *Student Member, IEEE*, James L. Drewniak, *Member, IEEE*, Todd H. Hubing, *Senior Member, IEEE*, Thomas P. Van Doren, *Senior Member, IEEE*, and Richard E. DuBroff, *Senior Member, IEEE*

Abstract—Stacked-card and modules-on-backplane printed circuit-board geometries are advantageous for conserving real-estate in many designs. Unfortunately, at high frequencies, electromagnetic interference (EMI) resulting from the nonnegligible impedance of the signal return at the connector may occur. This effective EMI coupling path results in the daughtercard being driven against the motherboard and attached cables, resulting in common-mode radiation. The connector geometry can be modified to minimize the EMI coupling path when high frequencies are routed between the motherboard and daughtercard. Current speeds and printed circuit board (PCB) sizes result in geometries that are of significant dimensions in terms of a wavelength at the upper frequency end of the signal spectrum. The PCB geometries are then of sufficient electrical extent to be effective EMI antennas. The resonant lengths of the EMI antennas may, however, be quite removed from the typical half-wavelength dipole resonances. The finite-difference time-domain method can be used to numerically analyze the printed circuit-board geometries, determine antenna resonances, and investigate EMI coupling paths. EMI resulting from the stacked-card configuration has been investigated experimentally and numerically to ascertain the EMI coupling path at the bus connector, and EMI antennas.

Index Terms—Electromagnetic coupling, electromagnetic interference (EMI), finite difference time domain (FDTD) methods, impedance measurement, poles, printed circuit layout, zeros.

I. INTRODUCTION

THE evolution of the electronics industry has placed size minimization among the primary attributes in emerging product designs. Stacked-card and modules-on-backplane printed circuit board (PCB) configurations have proven to be successful methods for conserving real-estate. Unfortunately, noise can be coupled throughout the system as a result of connector parasitics. Mechanisms by which differential-mode signals are converted to common-mode noise sources resulting in electromagnetic interference (EMI) have been demonstrated experimentally [1]–[3]. Two classes of coupling mechanisms are voltage-driven and current-driven [1]. The current-driven mechanism is of particular importance for PCB connector geometries, and is reviewed herein for this application.

Fig. 1 shows a two-dimensional (2-D) view of a stacked-card configuration with a daughtercard and motherboard. A trace is routed along the motherboard and onto the daughtercard where it is terminated. The signal-return path between the daughtercard reference plane and the motherboard reference plane is a conductor segment located some distance from the signal conductor. Another return path may be considered the "EMI antenna" current path depicted in the figure as a capacitor (displacement current). The connection between the daughtercard and motherboard is comprised of a large loop, where the magnetic flux shown in Fig. 1 is predominantly circling the signal conductor, and the signal-return conductor. The flux wrapping the signal-return conductor results in an effective EMI noise source between the daughtercard and the motherboard (assuming the height is electrically small), and is referred to as a current-driven coupling mechanism. Typically, the impedance of the EMI antenna is large, and little common-mode current is driven onto the antenna. However, when the geometry is of resonant dimensions, the impedance of the EMI antenna may be less than 100 Ω, and the induced common-mode currents can result in radiation. The flux that wraps the signal-return connector can be modeled as a partial inductance [4]. By constructing a connector that minimizes the partial inductance of the signal-return conductor, the effect of a current-driven EMI coupling mechanism at the connector can be reduced.

The EMI antennas on the PCB for the stacked-card configuration are not easily characterized. The antenna does not usually consist of simply wires and cables. Consequently, finding the frequency for which the "length" of the antenna is a half-wavelength is inadequate for the first resonance frequency. Intuitively, the presence of a large plate as one of the conductors provides more capacitance to the antenna, thereby shifting the resonances lower in frequency. These structures can be modeled with the finite-difference time-domain (FDTD) method, and the resonance frequencies for complicated PCB geometries can be calculated.

II. STACKED-CARD CONFIGURATION

The connector geometry linking a daughtercard and motherboard must be carefully designed to accommodate the
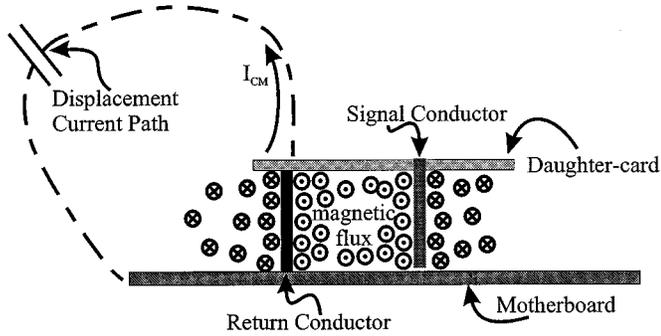
Fig. 1. Cross section of a stacked-card PCB configuration showing the magnetic flux coupling the EMI antenna path.

bandwidth associated with the signals transmitted through the connector. The modules-on-backplane configuration has been numerically studied using the FDTD method with reasonable agreement with experimental results [5]. The EMI associated with a stacked-card PCB design was studied here through the common-mode current induced on a cable attached to the motherboard. For stacked-card PCB designs, EMI coupling paths result from a variety of layout and design features. Fig. 2 shows a few relevant examples found on typical stacked-card designs. For example, the heat-sink on the microprocessor may be driven by parasitic capacitive coupling from the IC or a nearby trace, the nonzero impedance of the motherboard or daughtercard reference plane signal return paths may result in a current-driven mechanism [3], [6], and the bus connector may result in a current-driven mechanism. Test geometries were developed to experimentally and numerically study EMI resulting from the nonzero impedance of the bus connectors between daughtercards and motherboards.

A test configuration with traces on the motherboard and daughtercard is shown in Fig. 3. The traces are 2 mm wide and 1.5 mm above the reference planes. The reference planes are constructed of electro-deposited copper on an FR4 dielectric substrate. The cable extending from the motherboard is 0.085-in semirigid coaxial cable. The cable is connected to the bottom of the motherboard and penetrates the motherboard at the trace origin 10 cm from the right PCB edge. The shield of the coaxial cable is soldered to the motherboard with a 360° connection, where it penetrates the plane at the signal trace. The shield is also soldered to the ground plane along its length. The center conductor of the coaxial cable is extended through the motherboard and connected to the trace. The trace is routed to the connector. A 24-AWG wire is used as the signal-current conductor between the motherboard trace and the daughtercard trace. The signal-current conductor is located at the center of the connector edge of the daughtercard as shown in Fig. 3. The daughtercard trace is routed 8 cm along the daughtercard and shorted to the daughtercard reference plane. A 24-AWG wire is used for the signal-return conductor a distance d from the signal conductor. The wire is soldered to the daughtercard and the motherboard reference planes. The signal-input end of the coaxial cable is connected to an SMA bulkhead through mounted in a 60 cm×60 cm aluminum plate. The bulkhead connector provides a 360° connection to the aluminum plate. The aluminum plate is used to isolate the stacked-card model from

the cable dressing leading to the HP8753D network analyzer. A Fischer F-2000 clamp-on current probe (100 MHz–3000 MHz) was mounted adjacent to the aluminum plate and encircled the feeding coaxial cable. The probe was not specified to 10 MHz, however the transfer impedance of the probe was sufficient between 10 MHz and 100 MHz to measure the common-mode current. A ferrite sleeve (100 Ω at 100 MHz) was mounted around the probe connector to reduce coupling to the current probe. The bus-connector test configuration is located at the edge of the daughtercard as opposed to slightly removed from the card edge, as is typically the case in manufactured boards, in order to facilitate changes in the connector geometry for the experiments. Often, stacked-card configurations for high-speed designs are placed in shielding enclosures. In these cases, common-mode current on motherboards, daughtercards, and cables resulting from parasitics at the bus connector may couple to another internal device, or the chassis enclosure modes, and radiate through apertures or on I/O lines driven against the chassis.

An HP8753D network analyzer was used to measure S_{21} with the locations of Port 1 (the voltage source for the signal trace) and Port 2 (current-probe on the cable) as shown in Fig. 3. A small copper ring was used to calibrate the network analyzer and remove the frequency response of the current-probe. The copper ring was wrapped tightly around the current-probe and connected to Port 1 during calibration. The current in the copper ring at frequencies where the source impedance is significantly greater than the calibration ring loop inductance was

$$I_{\text{Port 1}} \approx \frac{V_S}{50} \qquad (1)$$

where

$I_{\text{Port 1}}$ is the current in the copper loop,
V_S is the RF source voltage of the network analyzer, and
50 Ω   was the source impedance of the network analyzer.
The voltage at Port 2 was

$$V_2^- = 50 \, I_{\text{Port 2}} \qquad (2)$$

where $I_{\text{Port 2}}$ was the current sensed by the current probe. The currents in Port 1 and Port 2 were related by the transfer impedance of the current probe $Z_T(f)$, therefore $I_{\text{Port 2}} = (Z_T(f)/50)I_{\text{Port 1}}$. The voltage wave incident on Port 1 was $V_1^+ = V_S/2$, because the 50-Ω source impedance was matched to the characteristic impedance of the cables. Before calibration, S_{21} was then

$$|S_{21}| = \left| \frac{V_2^-}{V_1^+} \right| = \left| \frac{50 \dfrac{Z_T(f)}{50} \dfrac{V_S}{50}}{\dfrac{V_S}{2}} \right| = \left| 2 \frac{Z_T(f)}{50} \right|. \qquad (3)$$

Therefore, the calibration procedure removed the factor $2(Z_T(f)/50)$. Consequently, the $|S_{21}|$ was related to the common-mode current by

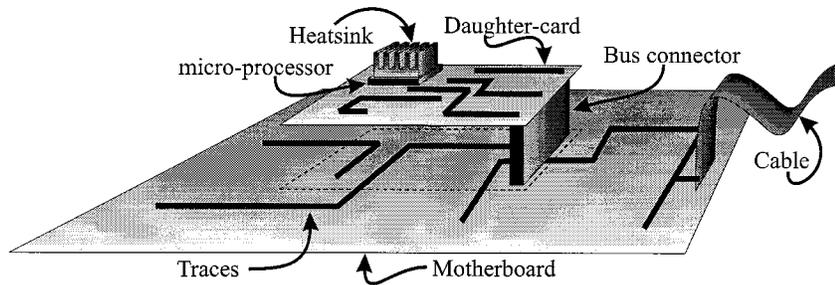$$|S_{21}| = 50 \left| \frac{I_{CM}}{V_S} \right|. \qquad (4)$$

Fig. 2.   Representation of a general stacked-card geometry. EMI may result from coupling to heat-sinks, finite-impedance reference structures, or bus connectors.
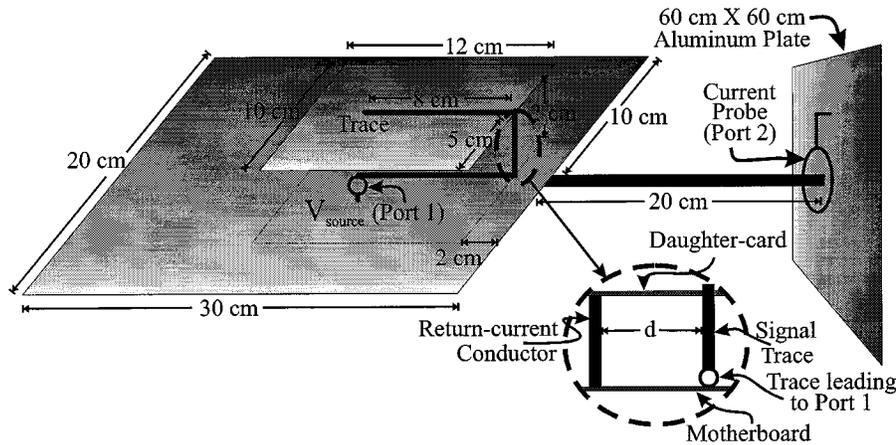

Fig. 3.   Stacked-card model with traces. The connector region is exploded to show the separation between the signal conductor and the return conductor.
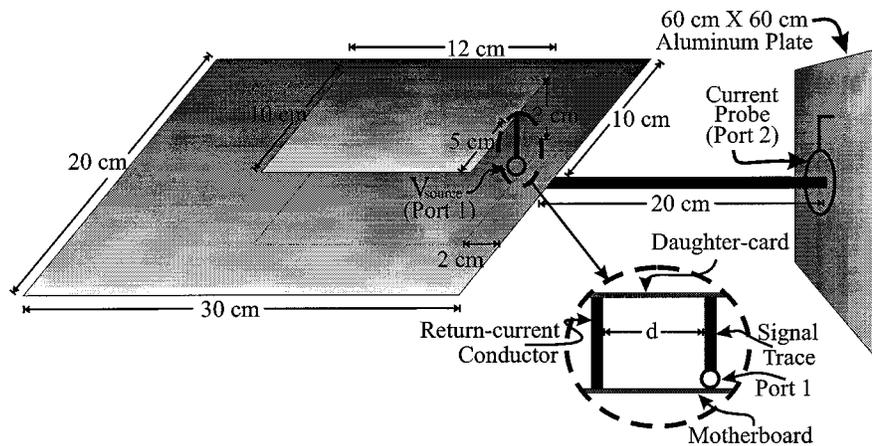

Fig. 4.   Stacked-card model without traces. Connector region is exploded to show the separation between the signal conductor and the return conductor.

Equation (4) was used to compute $|S_{21}|$ for comparisons between the experimental and numerical results.

The configuration depicted in Fig. 3 shows a trace geometry that begins on the motherboard, is routed onto the daughter-card, and then terminated in a short circuit. Swept-frequency measurements were conducted between 10 MHz and 1 GHz. The trace geometry was 16 cm long, which is significant compared to a wavelength at frequencies beyond 120 MHz. Consequently, the current distribution is no longer uniform along the trace. It is difficult with the model including the trace geometry shown in Fig. 3 to investigate the EMI resulting from the connector geometry, because the current in the connector

conductors changes as the standing wave pattern changes over a significant portion of the measurement frequency range. A model neglecting the trace geometry is desirable to investigate the role of the bus connector as an EMI coupling path if the trace geometry has little impact on the resulting EMI. Measurements on the configuration shown in Fig. 4 with the trace geometry omitted were compared for that of Fig. 3 to determine the significance of the trace geometry on the EMI mechanism. In the configuration without the trace, Port 1 was located between the motherboard and the signal conductor in the connector. The signal conductor was terminated directly to the daughtercard. The connector was 2 cm tall, which was less

than one tenth of a wavelength at 1 GHz. The current is then approximately constant along the connector conductors.

$|S_{21}|$ was measured for the geometries in Figs. 3 and 4 and the results are shown in Fig. 5 for signal and return separations of $d = 5$ cm. The common-mode current increases at approximately 12 (dB/octave) below the first resonance, as expected for a current-driven mechanism [1]. For the case of $d = 2$ cm, which is not shown in the figure for clarity, the resonances occur at approximately the same location since they are determined by the EMI antenna geometry, although $|S_{21}|$ of the resonances differs slightly. The difference in the measured $|S_{21}|$ (proportional to $|I_{CM}|$) is due to changes in the connector geometry, which changes the current distribution.

The signal geometry can be modeled as two transmission lines connected by a lumped-element inductance up to 1 GHz. One transmission line represents the microstrip on the motherboard, the other the microstrip on the daughtercard. The connector can be modeled approximately as a lumped-element inductance. Given the dimensions and materials of the microstrip geometry, the effective relative-dielectric constant was $\epsilon_e = 3.44$ and the characteristic impedance was $Z_o = 60\ \Omega$ [7]. The inductance of the connector loop was measured using an HP4912A impedance/material analyzer to be $L \approx 58$ nH when the signal-return conductor was located 5 cm from the signal-current conductor.

The input impedance at the input terminals on the motherboard for the resulting transmission-line model has poles at approximately 180 MHz and 600 MHz, and zeros at 500 MHz and 650 MHz. The first pole results in little current being driven onto the microstrip. The $|S_{21}|$ for the stacked-card configuration with a trace show less measured common-mode current around 180 MHz, because less differential-mode current results in a smaller current-driven coupling mechanism. Similarly, the zero at 500 MHz is a resonance that has a low magnitude of current at the center of the transmission line. Therefore, less current is conducted at the connector to excite the current-driven mechanism. Less common-mode current results as shown in Fig. 5 when the traces are included than when the traces are omitted. However, the nulls or common-mode current minima are the signal (microstrip) transmission-line resonances. The peaks of common-mode current shown in Fig. 5 are the result of EMI antenna resonances associated with the large reference conductors, rather than transmission-line resonances associated with the trace geometry.

The presence of the traces complicates the model, because the current-distribution on the microstrip traces changes with frequency. This study focuses on the relationship between the current in the connector, and the resulting common-mode current on the cable. The connector height is small relative to a wavelength at 1 GHz, and the impedance for the loop ($d = 5$ cm) is less than 50 Ω. Consequently, the current in the connector changes minimally over the measured frequency range. Conversely, for the model shown in Fig. 3, where the trace geometry is included, the input impedance of the transmission-line geometry fluctuates between low and high impedance values in the range 10 MHz to 1 GHz, and, therefore, the magnitude of the current at the connector is varying with frequency. By removing the trace, the EMI coupling path at the connector can
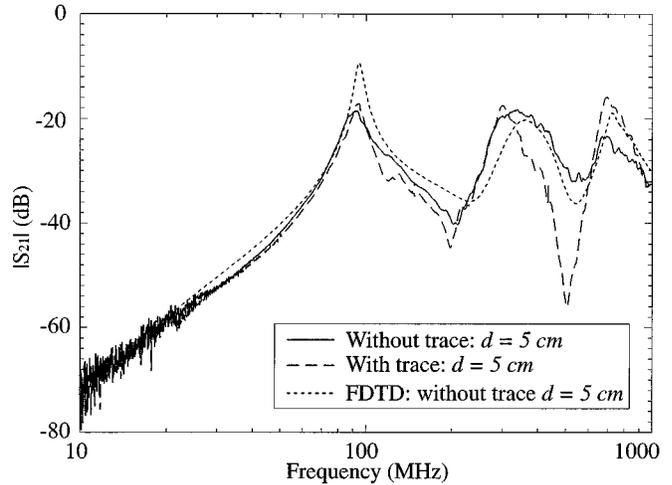

Fig. 5. Comparison of $|S_{21}|$ experimental results for a stacked-card model with and without a trace geometry, and FDTD results for the stacked-card model without a trace.

be more closely studied. Therefore, the model shown in Fig. 4 was chosen as the test-bed for this analysis. Ultimately, models generated from the bus-connector investigation might be used in conjunction with transmission line models and available IC models to predict EMI levels.

The FDTD method was used to numerically investigate the stacked-card configuration. Details of the FDTD method can be found in [8] and [9]. The geometry shown in Fig. 4 was modeled with cubic cells 1 cm on a side, and a time step $\Delta t = 16.67$ ps. The planes were modeled as perfect-electric conductors (PECs), and the wire and cable conductors were modeled with a thin-wire algorithm [10], [11]. Only the conductors shown in Fig. 4 were modeled. The current probe was not modeled in the numerical studies. The source was a 50-Ω modulated-sinc function with a radius modeled in a similar fashion as the wire [12]. Perfectly matched layer (PML) absorbing boundaries were used to truncate the computational domain eight cells from the conductors [13]. Six PML layers were employed.

The FDTD results shown in Fig. 5 agree favorably with the experimental results (without traces) up to 1 GHz. The agreement for the case of $d = 2$ cm (not shown in the figure) is also good. The omission of conductor loss in the FDTD model results in higher peaks at resonances than in the experimental data, but the frequency variations are the same. The primary discrepancy between the FDTD and experimental results shown in Fig. 5 is the difference in $|S_{21}|$ as the frequency increases. The problem results from complications in the experimental data rather than the numerical model. A small calibration ring is used during calibration to remove the frequency response of the current probe. The calibration ring fits tightly around the current probe, however, the inductance of the ring becomes appreciable compared to 50 Ω as the frequency increases. Including the calibration ring inductance in determining the numerical $|S_{21}|$ improves the agreement between the numerical and experimental results to approximately 700 MHz, however the error around the third resonance peak increases. One possible reason for the increase in error around the third $|S_{21}|$ peak is coupling to the current-probe housing. The ferrite sleeve may not provide much impedance
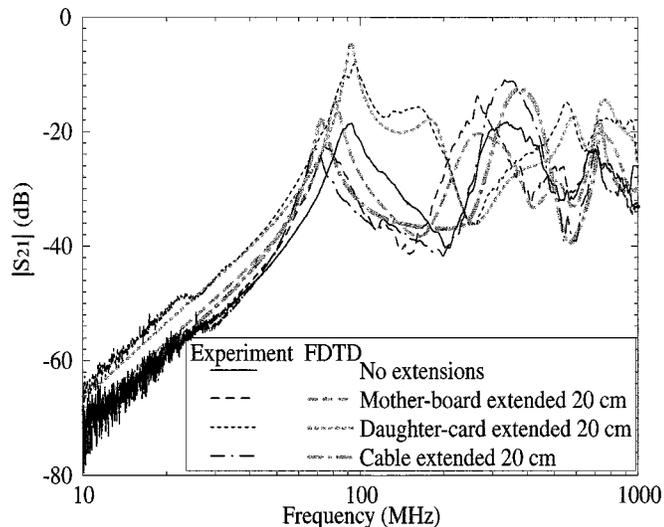
Fig. 6. $|S_{21}|$ results for the stacked-card configuration with $d = 5$ cm and no extended conductors, a 20-cm motherboard extension, a 20-cm daughtercard extension, and a 20-cm cable extension.

Fig. 7. $|S_{21}|$ results for signal- and return-conductor separations of $d = 5$ cm, 2 cm, 2 mm, and a microstrip-style connector.

near 1 GHz, therefore, electric flux lines can terminate on the current probe and current through this path can be conducted back to the source without being measured with the probe.

III. EXPERIMENTAL AND NUMERICAL RESULTS

There are three maxima in the results shown in Fig. 5 from 10 to 1000 MHz. These resonances result from complex interactions between various conductors comprising specific EMI antennas. Within a limited frequency range around each resonant maximum, a particular EMI antenna geometry dominates. Three possible EMI antennas are the daughtercard being driven against the cable, the motherboard being driven against the cable, and the daughtercard being driven against the motherboard. Each resonance was analyzed in detail and the dominant EMI antenna structures were identified. Differential-mode energy is converted to common-mode energy because of the finite impedance of the signal-return conductor connecting the two planes. The signal-return conductor was also changed to show how lowering the impedance of the signal-return path may reduce EMI.

A. First Resonance

The first resonance is at approximately 90 MHz. The finite impedance of the signal-return conductor was the EMI coupling mechanism, and the experimental configuration was altered to identify the EMI antenna. The cable, daughtercard, and motherboard were alternately extended 20 cm. From antenna theory, extending the conductors should shift the resonance lower in frequency if the extended conductor is a primary component in the antenna [14]. The $|S_{21}|$, which is proportional to the common-mode current on the cable, is shown in Fig. 6.

The first resonance shifted lower in frequency when the cable was extended, indicating that the cable was part of the EMI antenna. However, the resonance did not shift when the daughtercard was extended, although $|S_{21}|$ increased in magnitude. The resonance also shifted lower in frequency when
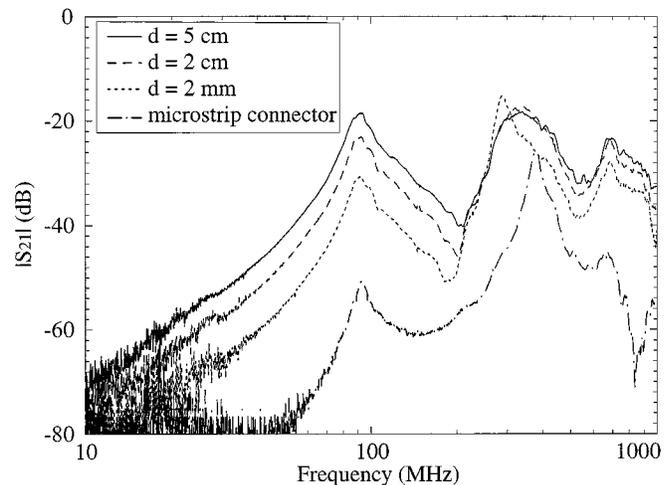
the motherboard was extended. Therefore, the primary EMI antenna was the motherboard and cable for the first resonance. The EMI resulted from the finite impedance of the signal-return conductor, and energy was capacitively coupled to the EMI antenna. The daughtercard over the motherboard was effectively a parallel plate capacitor. The displacement-current path from the daughtercard to the motherboard excited the EMI antenna. An analogous antenna array geometry would be a short nonresonant driven dipole parasitically coupling to a shorted resonant dipole in proximity. Consequently, when the daughtercard was extended, the coupling to the EMI antenna increased, although the resonance frequency of the antenna did not shift.

FDTD results for the stacked-card configuration with extended conductors are also shown in Fig. 6. For the case with no extensions, the FDTD result is shown in Fig. 5. The experimental and numerical results agree favorably over the entire frequency range. One cause for the discrepancies is the conductor loss. The numerical results are greater at resonant peaks, because the conductors were modeled as PECs, whereas the physical conductors have loss. Secondly, the dimensions of the experimental model are not precisely the same as the dimensions in the numerical model, because of machining tolerances.

The EMI antenna in the frequency band around the first resonance was comprised of the motherboard and cable. Differential-mode energy was converted to common-mode energy because of the finite-impedance of the signal-return conductor. This impedance could be lowered by reducing the distance d between the signal and return conductors. The $|S_{21}|$ results for separations of $d = 5$ cm, 2 cm, and 2 mm are shown in Fig. 7. Reducing the separation from 5 cm to 2 cm reduced the common-mode current by approximately 5 dB below 200 MHz. The common-mode current was reduced by approximately 12 dB when the separation was reduced from 5 cm to 2 mm. The impedance of the signal return may also be reduced by widening the return conductor, such as in a microstrip configuration. A 2.5 cm wide copper strip was centered 2 mm behind the signal conductor and connected to the daughtercard and motherboard. A 30-dB reduction in common-mode current is shown in Fig. 7 below 200 MHz when
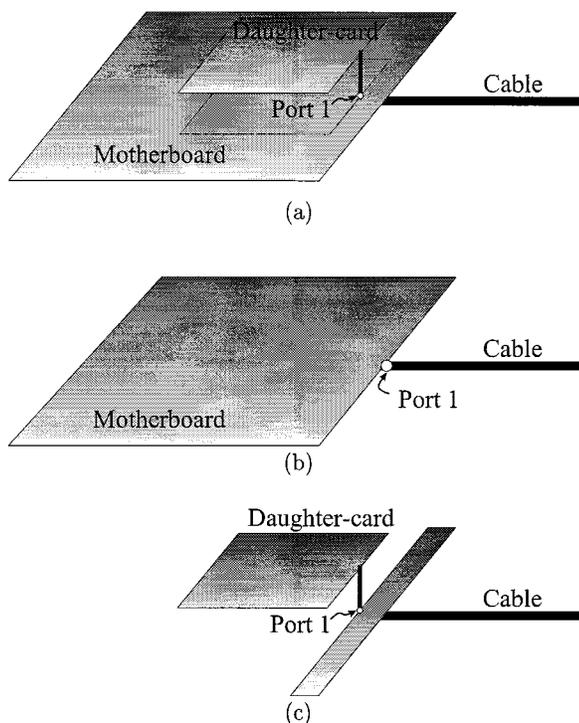
Fig. 8.   Schematic representation of the modified EMI antennas: (a) daughtercard and motherboard, (b) motherboard and cable, and (c) daughtercard and cable. Port 1 shows the location of the effective antenna terminals for impedance measurements.

the return conductor is changed from a wire 5 cm from the signal conductor to the microstrip-style connector. Numerical results were also generated for these cases, with agreement to the modeling similar to the previous cases.

B. Second Resonance

The second resonant maximum in the common-mode current results of Fig. 6 occurs at approximately 350 MHz. The relevant antenna at the second resonance was investigated by extending the conductors and measuring $|S_{21}|$. Extending the cable resulted in greater common-mode current, but did not shift the resonance. This change will be explained below when EMI antenna input impedance is discussed. Extending the motherboard and daughtercard resulted in a lower resonance frequency, although other peaks shifted lower in frequency in proximity to 350 MHz. Therefore, the EMI antenna in the frequency band around the second resonance included the daughtercard and motherboard. However, the common-mode current was measured on the cable, which must then be part of the EMI antenna. Input impedance measurements and modeling provided further insight regarding the second resonance.

An HP4912A impedance/material analyzer (1 MHz–1.8 GHz) was used to measure the input impedance for the three EMI antennas. Schematic representations of the three antenna geometries are shown in Fig. 8. The motherboard and cable EMI antenna was evaluated by placing the antenna terminals between the motherboard and the cable. The daughtercard geometry was removed from these measurements. The daughtercard and cable antenna was evaluated by truncating the motherboard at the connector. The antenna terminals were

place at Port 1 as shown in Fig. 8(c). The motherboard and daughtercard EMI antenna was investigated by analyzing the stacked-card geometry without a signal-return conductor. The EMI antenna was mounted on the aluminum plate as shown in Fig. 4 for all three EMI antenna input-impedance experiments. The results for the input impedance of the three EMI antennas are shown in Fig. 9. Relevant conductors in each EMI antenna were extended, and the changes in input impedance determined. The motherboard and daughtercard input-impedance results are shown in Fig. 9(a). The resonance at approximately 300 MHz results from the parallel-plate transmission-line configuration of the daughtercard and motherboard. The length of the transmission line was dominated by the daughtercard. Fringing fields may have terminated on the portion of the motherboard beyond the daughtercard, but extending the motherboard did not shift the resonance, as shown in Fig. 9(a). However, extending the daughtercard shifted the resonance lower in frequency toward 100 MHz.

The input impedance at the connector between the motherboard and daughtercard is approximately 1 Ω, at the quarter-wavelength resonance. This resonance resulted in significant levels of current returning to the source through the resonant transmission-line, as opposed to the dedicated signal-return conductor. The magnetic flux associated with the high currents wrapped the motherboard, which excited the motherboard and cable [6]. The resonance is a result of the parallel-plate quarter-wavelength resonance, however, the common-mode current increased at the second peak when the cable was extended, as shown in Fig. 6. The common-mode current increased, because extending the cable resulted in a series-type resonance near 300 MHz, as shown in Fig. 9(b). Consequently, the common-mode current for the test configuration in Fig. 4 increased at the second resonance when the cable was extended, as illustrated in Fig. 6. Furthermore, when the motherboard was extended, a series-type resonance occurred near 250 MHz as shown in Fig. 9(b). The combination of the high currents on the motherboard and the resonance at 250 MHz shifted the second common-mode current peak of Fig. 6 lower in frequency when the motherboard was extended.

The results for the daughtercard and cable antenna are shown in Fig. 9(c). The resonances associated with the daughtercard and cable antenna did not appear to affect the common-mode current shown in Fig. 6 significantly. This may indicate that the daughtercard and cable EMI antenna was too closely coupled to the other two antennas to be excited independently.

FDTD results are also presented in Fig. 9 for comparison with the experimental results. The results agree reasonably well to 1 GHz, except when the cable was extended 20 cm. The calibration reference-plane was not exactly at the same point for the numerical model and experimental model, because of machining difficulties. The differences in the location of the calibration reference-plane may be the cause of the discrepancies.

The common-mode current induced on the cable at the second resonance resulted from the high currents conducted along the daughtercard and motherboard near the motherboard and daughtercard transmission-line resonance. The current on the motherboard results in a magnetic field that couples the motherboard and cable EMI antenna. Lowering the partial

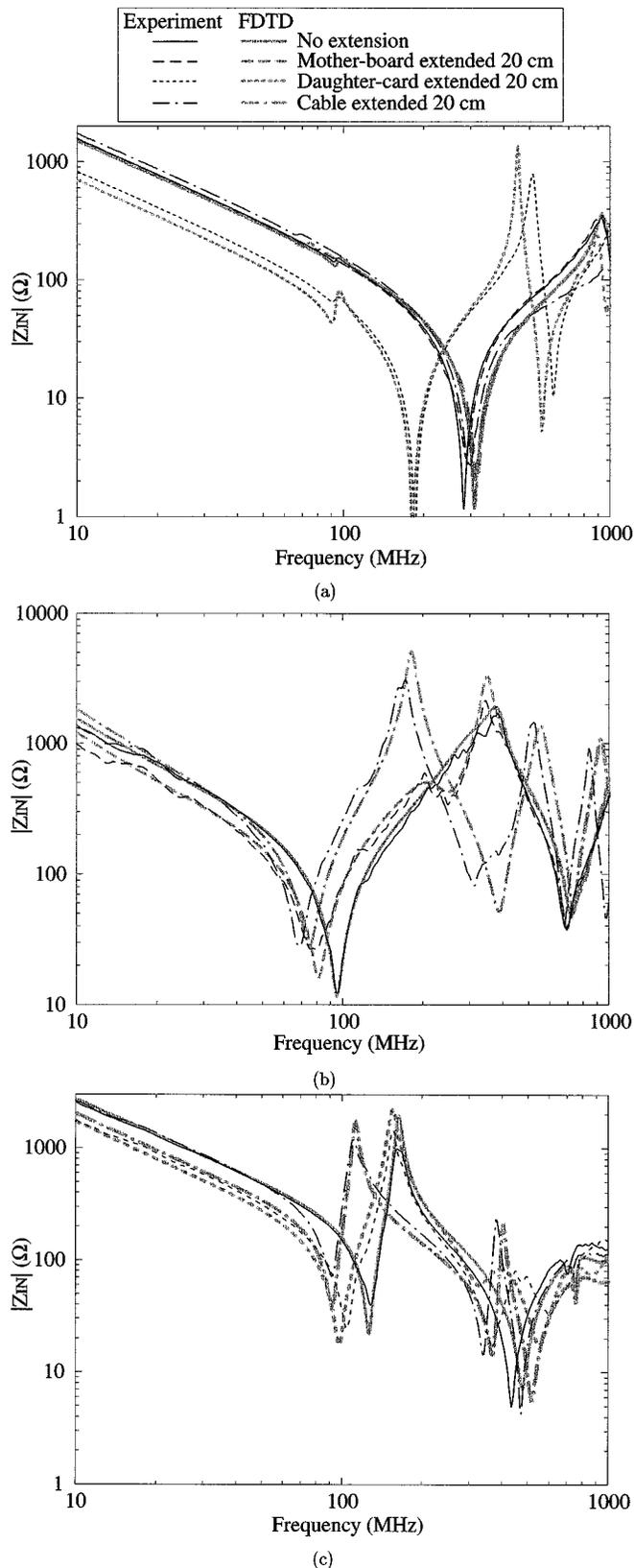| Experiment	FDTD	
——	——————	No extension
– – –	— – — –	Mother-board extended 20 cm
········	··········	Daughter-card extended 20 cm
—·—	—·——·—	Cable extended 20 cm

(a)

(b)

(c)

Fig. 9. Magnitude of the input impedance for the three EMI antenna configurations: (a) daughtercard and motherboard, (b) motherboard and cable, and (c) daughtercard and cable.

inductance of the signal-return conductor in the connector reduced the noise significantly at the first resonance, because the

improved connector geometry provided a low-impedance path for currents to return to the source. Unfortunately, the second resonance resulted from a very low impedance parasitic-return path. Reducing the partial inductance of the signal-return conductor did not significantly lower the common-mode current on the cable, because it was difficult to provide a lower impedance than the motherboard and daughtercard impedance at this transmission-line resonance. The best reduction in noise, achieved with the microstrip-style connector, was approximately 6 dB at the second peak, as shown in Fig. 7.

C. Third Resonance

The third peak in common-mode current for the stacked-card configuration occurred at approximately 700 MHz, as illustrated in Fig. 6. The resonant antenna was determined by evaluating each EMI antenna independently. Fig. 9(b) shows the input impedance of the motherboard and cable EMI antenna with antenna terminals between the motherboard and the cable. A series-type resonance occurred at approximately 700 MHz. A resonance is evident at 700 MHz when the motherboard and cable conductors were extended, as well. As shown in Fig. 9(b), extending the motherboard does not change the impedance near 700 MHz, perhaps because the motherboard is already so large at 700 MHz that extending the motherboard further is ineffective. A new resonance is shifted to 700 MHz when the cable is extended, however, the input impedance on either side of the resonance is increased, as shown in Fig. 9(b).

A small resonance near 700 MHz also occurs in the daughtercard and cable antenna, as illustrated in Fig. 9(c), but it is inconsistent with the $|S_{21}|$ results shown in Fig. 6. Extending the cable lowered the input impedance of the daughtercard and cable EMI antenna, which should have resulted in an increase in common-mode current. However, the common-mode current decreased near the third resonance when the cable was extended, as depicted in Fig. 6. Conversely, the impedance of the motherboard and cable EMI antenna on either side of the third common-mode current peak increased when the cable was extended, as shown in Fig. 9(b). Extending the cable should therefore result in lower common-mode current, which is consistent with Fig. 6. Another resonance was shifted down to approximately 650 MHz when the daughtercard was extended as indicated in Fig. 9(a). Consequently, another resonance at 650 MHz is seen in Fig. 6 when the daughtercard was extended, although the original resonance at 700 MHz remained. At high frequencies, the EMI antennas are closely coupled, and it is difficult to determine the dominant EMI antenna as unequivocally as with the other two common-mode current peaks. However, the common-mode current and input-impedance results at the third maximum support the motherboard and cable EMI antenna as the dominant EMI antenna.

The impedance of the signal-return path was relatively unaffected by changing the bus-connector, unless the spacing between the signal and return conductors was reduced to 2 mm. The input-impedance results for the four bus-connector configurations ($d = 5$ cm, 2 cm, 2 mm, and the microstrip-style connector) are shown in Fig. 10 measured with terminals at Port 1 as shown in Fig. 4. The pole-zero pair near 300 MHz results from the parallel combination of the inductance of the
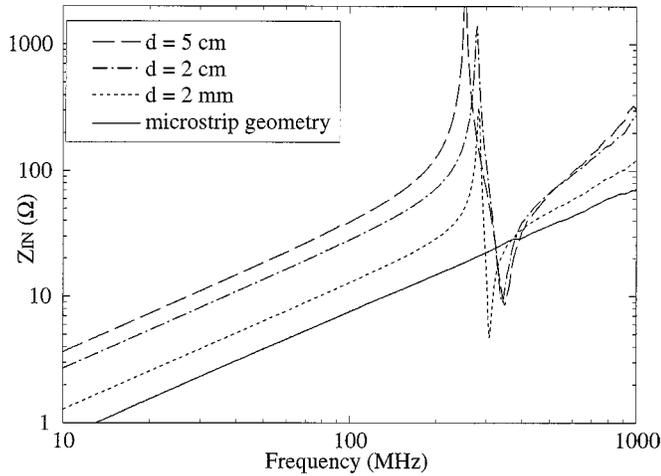
Fig. 10. Measured magnitude of the input impedance at Port 1 for the stacked-card configuration with signal-return conductor separations $d = 5$ cm, 2 cm, 2 mm, and a microstrip-style connector.

connector, and the parallel-plate transmission-line of the motherboard and daughtercard. The impedance of the connector was essentially unchanged at frequencies above 400 MHz until the signal-return conductor separation was reduced to 2 mm. The impedance of the signal-return wire may be approximated as half of the total impedance, assuming that the magnetic flux in the connector loop wraps the wire conductors and not the large plate conductors. Reducing the impedance of the connector results in a reduction in the EMI coupling path. Consequently, the common-mode current was relatively unchanged near the third resonance until the signal-return conductor separation was reduced to 2 mm, as shown in Fig. 7.

A 30-dB reduction in common-mode current was achieved by reducing the impedance between the daughtercard and the motherboard reference planes with a microstrip-style connector. As illustrated in Fig. 10, the total connector impedance was reduced by only 4 dB when the microstrip-style connector was employed, as compared to the connector configuration where the signal-return was 2 mm from the signal conductor. However, the partial inductance of the signal-return conductor associated with the magnetic flux wrapping that conductor leads to radiated EMI [6]. The majority of the magnetic flux in the microstrip-style connector wrapped the signal conductor. Therefore, the impedance of the signal-return structure, and, consequently, the EMI, was significantly reduced. The reduction of the signal-return impedance may also be considered as magnetic-flux containment. A signal return geometry that cannot be wrapped by magnetic flux, like a coaxial shield, should minimize coupling between the connector and the EMI antennas for frequencies where the magnetic-field is the dominant EMI coupling mechanism.

D. Multiple Return-Current Conductors

Multiple signal-return conductors are often used in bus connectors for impedance control. Although the primary reason for using multiple reference conductors in the bus is to improve signal integrity, multiple conductors result in a lower signal-re-
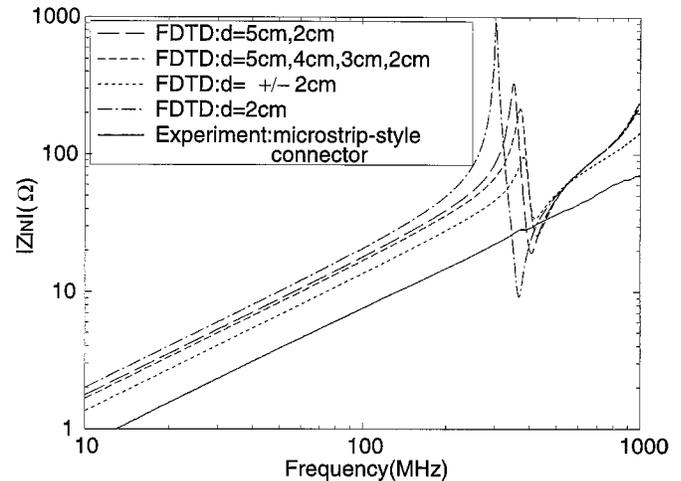
(a)
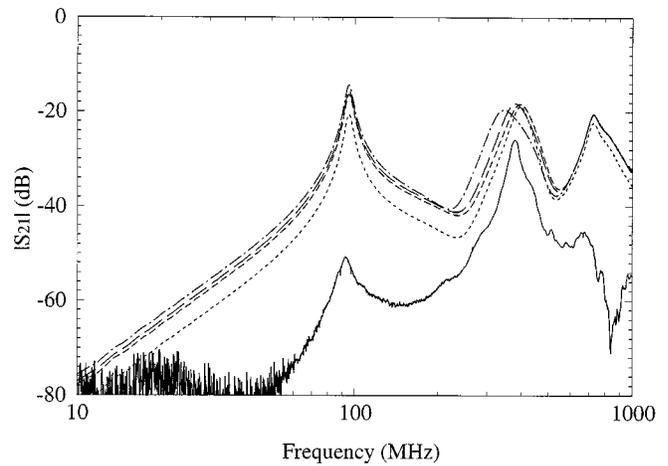
(b)

Fig. 11. (a) Input-impedance and (b) $|S_{21}|$ numerical results for the stacked-card configuration with return conductors 5 cm and 2 cm from the signal conductor, 5 cm, 4 cm, 3 cm, and 2 cm from the signal conductor, 2 cm on both sides of the return conductor, 2 cm from the return conductor, and experimental results for the microstrip-style connector.

turn impedance that may reduce EMI. FDTD was used to investigate the changes in the EMI performance of a bus connector with multiple signal-return conductors.

Three multiple signal-return conductor configurations were investigated. The stacked-card geometry with two signal-return conductors (5 cm and 2 cm from the signal conductor), four signal-return conductors (5 cm, 4 cm, 3 cm, and 2 cm from the signal conductor), and two symmetrically located signal-return conductors (2 cm from both sides of the signal conductor) were modeled with FDTD. The input impedance and $|S_{21}|$ results for the multiple signal-return configurations are shown in Fig. 11. Numerical results for the bus-connector with a return conductor 2 cm from the signal and the experimental results for the microstrip-style connector are included as a reference.

The total inductance of the signal-return loop at the bus connector was reduced by 1 dB when multiple signal-return conductors were used on only one side of the signal conductor, as shown in the input-impedance results of Fig. 11(a). Placing the reference conductors on both sides of the signal conductor reduced the total inductance by 3.4 dB compared to the total inductance with

one signal-return conductor at 2 cm. The peaks of the resonances were less severe when multiple conductors are used.

The magnitude of the magnetic field around a wire declines rapidly with distance. The majority of the current flows on the signal-return conductor closest to the signal conductor. Consequently, the impedance of the signal-return path did not change significantly when multiple wire conductors were placed on one side of the signal conductor. The partial inductance of the signal returns may be significantly reduced when reference conductors are placed on both sides of the signal conductor, because the signal-return current will be more uniformly distributed [15]. Fig. 11(b) shows that the common-mode current was reduced by no more than 2 dB when multiple signal-return conductors were placed on one side of the signal conductor. By symmetry, the impedance of the signal-return path is reduced by a factor of two when the signal-return conductors are placed on both sides of the signal conductor. Therefore, the common-mode current was reduced by 6 dB below 200 MHz (and away from antenna resonances) when signal-return conductors were placed on both sides of the signal conductor, as compared to one signal-return conductor placed 2 cm from the signal conductor.

Multiple signal-return conductors did not significantly reduce EMI in the stacked-card model beyond 500 MHz. The impedance of the wire conductors above 500 MHz was much higher than the impedance of the motherboard and daughtercard parallel-plate transmission-line. Therefore, the common-mode current above 500 MHz was relatively unchanged unless the microstrip-style connector was employed, as shown in Fig. 11(b). However, as indicated previously, at the quarter-wave motherboard and daughtercard transmission-line resonance, the transmission-line impedance was sufficiently low that even a microstrip-style connector could not significantly decrease the common-mode current at 400 MHz.

IV. Conclusion

The stacked-card configuration is frequently used as a real-estate saving method in high-speed digital designs, and bus connectors are commonly used to connect different modules, such as a daughtercard and a motherboard. Connectors must be carefully designed so reference planes on different modules are not driven against each other as an EMI antenna. A poor connector may be an effective current-driven EMI coupling path that could drive extended-reference conductors as EMI antennas. Other similar configurations such as modules-in-backplanes can lead to similar EMI problems.

Experimental and numerical models were constructed to analyze the EMI associated with the stacked-card PCB configuration. The signal-return conductor in the bus connector was the point of differential-mode to common-mode energy conversion resulting in EMI. In general, the EMI could be reduced 10 dB by placing the return conductor 2 mm from the signal conductor as opposed to 5 cm. By using a wide strip for the return conductor, the EMI could be further reduced 20 dB.

An improved connector geometry was realized by reducing the impedance of the signal-return conductors significantly with respect to the EMI antennas. Three maxima occurred in the common-mode current measured on the cable of the

stacked-card model below 1 GHz. The peaks resulted from complex interactions between reference conductors. However, the peaks could be associated with specific reference conductors in the model. The first and third peaks resulted from a resonant EMI antenna comprised of the motherboard and the attached cable. However, the second peak, near 350 MHz, resulted from a transmission-line resonance of the daughtercard and motherboard. At resonance, the daughtercard and motherboard parallel-plate transmission-line had a very low impedance. High currents were returned to the motherboard by the parasitic transmission-line structure, instead of the dedicated signal-return conductor. Establishing a dedicated low-impedance return path was more difficult near the second peak, because an unintentional low-impedance return path existed that resulted in EMI.

In general, larger signal-return conductors, such as in a microstrip geometry reduced the EMI. Multiple signal-return conductors may also reduce the impedance of the signal-return path, and FDTD was used to investigate the use of multiple signal-return conductors in the bus connector. The effective EMI coupling path was dominated by the signal-return conductor that was closest to the signal conductor. Multiple signal-return conductors placed on one side of the signal conductor resulted in no more than a 2-dB reduction in common-mode current compared to the results where the closest signal-return was used as the sole dedicated return-current path. Placing additional signal-return conductors on both sides of the signal conductor, however, reduced the common-mode current by approximately 6-dB below 200 MHz. Multiple signal-return conductors did not appear to significantly improve the EMI performance of the bus connector beyond 200 MHz, because the common-mode current was dominated by EMI antenna resonances.

References

[1] D. M. Hockanson, J. L. Drewniak, T. H. Hubing, T. P. Van Doren, F. Sha, and M. Wilhelm, "Investigation of fundamental EMI source mechanisms driving common-mode radiation from printed circuit boards with attached cables," *IEEE Trans. Electromagn. Compat.*, pp. 557–566, Nov. 1996.

[2] J. R. Bergervoet, "EMC measurements and models connecting the system level with the module level," *Phillips J. Res.*, vol. 48, pp. 63–80, 1994.

[3] F. B. M. van Horck, *Electromagnetic Compatibility and Printed Circuit Boards*. Eindhoven, The Netherlands: Tech. Univ. Eindhoven, 1998.

[4] A. E. Ruehli, "Inductance calculations in a complex integrated circuit environment," *IBM J. Res. Develop.*, vol. 16, pp. 470–481, 1972.

[5] K. Li, M. A. Tassoudji, S. Y. Poh, M. Tsuk, R. T. Shin, and J. A. Kong, "FD-TD analysis of electromagnetic radiation from modules-on-backplane configurations," *IEEE Trans. Electromagn. Compat.*, vol. 37, pp. 326–332, Aug. 1995.

[6] D. M. Hockanson, J. L. Drewniak, T. H. Hubing, T. P. Van Doren, F. Sha, C.-W. Lam, and L. Rubin, "Quantifying EMI noise sources resulting from finite-impedance reference planes," *IEEE Trans. Electromagn. Compat.*, pp. 286–297, Nov. 1997.

[7] D. M. Pozar, *Microwave Engineering*. Reading, MA: Addison-Wesley, 1990.

[8] A. Taflove, *Computational Electrodynamics: The Finite-Difference Time-Domain Method*. Boston, MA: Artech House, 1995.

[9] K. S. Kunz and R. J. Luebbers, *The Finite Difference Time Domain, Method for Electromagnetics*. Boca Raton, FL: CRC Press, 1993.

[10] K. R. Umashankar, A. Taflove, and B. Beker, "Calculation and experimental validation of induced currents on coupled wires in an arbitrary shaped cavity," *IEEE Trans. Antennas Propagat.*, vol. 35, pp. 1248–1257, Nov. 1987.